Chem. Senses 31: 425–435, 2006
doi:10.1093/chemse/bjj047
Advance Access publication March 17, 2006

Electrophysiological Properties and Modeling of Murine Vomeronasal Sensory Neurons in Acute Slice Preparations

Ranken Shimazaki[1], Anna Boccaccio[1], Andrea Mazzatenta[1], Giulietta Pinato[1], Michele Migliore[2,3] and Anna Menini[1]

[1]International School for Advanced Studies, SISSA, Sector of Neurobiology, Via Beirut 2-4, 34014 Trieste, Italy, [2]Institute of Biophysics, National Research Council, 90123 Palermo, Italy, and [3]Department of Neurobiology, Yale University, School of Medicine, New Haven, CT 06520, USA.

Correspondence to be sent to: Anna Menini, International School for Advanced Studies, SISSA, Sector of Neurobiology, Via Beirut 2-4, 34014 Trieste, Italy. e-mail: menini@sissa.it

Abstract

The vomeronasal system is involved in the detection of pheromones in many mammals. Vomeronasal sensory neurons encode the behaviorally relevant information into action potentials that are directly transmitted to the accessory olfactory bulb. We developed a model of the electrical activity of mouse basal vomeronasal sensory neurons, which mimics both the voltage-gated current properties and the firing behavior of these neurons in their near-native state, using a minimal number of parameters. Data were obtained by recordings with the whole-cell voltage-clamp or current-clamp techniques from mouse basal vomeronasal sensory neurons in acute slice preparations. The resting potential ranged from −50 to −70 mV, and current injections of less than 2–10 pA induced tonic firing in most neurons. The experimentally determined firing frequency as a function of injected current was well described by a Michaelis–Menten equation and was exactly reproduced by the model, which could be used in combination with future models that will include details of the mouse vomeronasal transduction cascade.

Key words: action potential, firing, mouse, pheromone, voltage-gated current, vomeronasal organ

Introduction

The vomeronasal system mediates responses to pheromones, molecules involved in communication and controlling specific behaviors, such as aggression, mating, and the recognition of gender and social status. The vomeronasal organ (VNO) of Jacobson is encased in a protective cartilaginous/bony capsule located above the palate in most mammals. Pheromones enter the lumen of the VNO, via a duct connecting it to the nasal or oral cavity, where they bind to receptors located on the microvilli on the dendritic knob of vomeronasal sensory neurons, bipolar cells which extend an axonal projection to the accessory olfactory bulb in the brain (for reviews on the vomeronasal system see Døving and Trotier, 1998; Jacobson *et al.*, 1998; Keverne, 2002; Zufall *et al.*, 2002, 2005; Dulac and Torello, 2003; Halpern and Martinez-Marcos, 2003; Rodriguez, 2003, 2004; Brennan and Keverne, 2004; Luo and Katz, 2004; Bigiani *et al.*, 2005).

Vomeronasal sensory neurons have been divided into two classes based on their location in the sensory epithelium and on the type of receptors they express. Apical neurons are located closer to the luminal space and express V1R and the G protein Gαi2, while basal neurons are located closer to the periphery of the sensory epithelium and express V2R and Gαo (Dulac and Axel, 1995; Berghard and Buck, 1996; Jia and Halpern, 1996; Herrada and Dulac, 1997; Matsunami and Buck, 1997; Ryba and Tirindelli, 1997). In the past few years considerable progress has been made in understanding how vomeronasal sensory neurons detect pheromones. Apical neurons are stimulated by small urine-derived volatile molecules (Leinders-Zufall *et al.*, 2000; Boschat *et al.*, 2002), while basal neurons are stimulated by a large family of nonvolatile peptide ligands of the major histocompatibility complex class I molecules (Leinders-Zufall *et al.*, 2004). Moreover, also odorants that are not pheromones can activate vomeronasal sensory neurons (Sam *et al.*, 2001; Trinh and Storm, 2003), although their physiological relevance is unclear. The detailed transduction pathway in vomeronasal sensory neurons is still largely unknown, but it has been shown that a transient receptor potential channel, TRPC2, is expressed in the microvilli (Liman *et al.*, 1999; Menco *et al.*, 2001) and that it is crucial for the

generation of electrical responses to pheromone stimulation (Leypold *et al.*, 2002; Stowers *et al.*, 2002; Lucas *et al.*, 2003; for a recent review see Zufall *et al.*, 2005). The signal transduction cascade, initiated by the binding of pheromones to vomeronasal receptors, produces an excitatory response. Indeed, it has been shown that natural stimuli cause membrane depolarization and increase the action potential firing rate in vomeronasal sensory neurons (Inamura *et al.*, 1997, 1999; Trotier *et al.*, 1998; Holy *et al.*, 2000; Inamura and Kashiwayanagi, 2000; Leinders-Zufall *et al.*, 2000, 2004; Taniguchi *et al.*, 2000; Boschat *et al.*, 2002; Cinelli *et al.*, 2002; Del Punta *et al.*, 2002; Spehr *et al.*, 2002; Lucas *et al.*, 2003).

How does an individual vomeronasal sensory neuron encode pheromone information into action potentials that are transmitted to the accessory olfactory bulb? Answering this question requires both the knowledge of the transduction machinery and of the mechanisms underlying action potential generation in individual vomeronasal sensory neurons. The goal of this study was to develop a model of the electrical activity of vomeronasal sensory neurons capable of reproducing the action potential firing, occurring after the activation of the vomeronasal transduction cascade, based on the properties of voltage-gated membrane ion channels.

The electrical properties of individual vomeronasal sensory neurons in the absence of chemical stimuli have been investigated with the patch-clamp technique in several studies, and it has been shown that these neurons are highly electrically excitable. Indeed, vomeronasal sensory neurons in some studies fired action potentials following depolarizing current injections of only 1–2 pA and, in addition, did not show sign of adaptation during small depolarizing current steps lasting up to 2 s (Trotier *et al.*, 1993; Liman and Corey, 1996; Inamura *et al.*, 1997). Voltage-gated ion channels have also been characterized in several voltage-clamp investigations and, although experiments showed a general agreement, some small differences were found among studies, possibly due to interspecies variability or different experimental protocols. Voltage-gated ion channel properties have been investigated in dissociated VNO preparations from frog (Trotier *et al.*, 1993; Trotier and Døving, 1996), mouse (Liman and Corey, 1996; Fieni *et al.*, 2003; Ghiaroni *et al.*, 2003; Dean *et al.*, 2004), lizard (Fadool *et al.*, 2001; Labra *et al.*, 2005), rat (Trotier *et al.*, 1998), and in VNO slice preparations from turtle (Taniguchi *et al.*, 1995, 1996), snake (Taniguchi *et al.*, 2000), and rat (Inamura *et al.*, 1997). Since many important recent advances in the knowledge of molecular mechanisms of vomeronasal transduction were obtained in the mouse (Holy *et al.*, 2000; Leinders-Zufall *et al.*, 2000, 2004; Lucas *et al.*, 2003), we developed a model of firing activity based on experiments on vomeronasal sensory neurons from the mouse. This model could be used in combination with future models that will include details of the vomeronasal transduction cascade. Since a recent study (Fieni *et al.*, 2003) has shown that mouse basal and apical neurons differ not only for their responses to pheromones (Leinders-Zufall *et al.*, 2000; 2004) but also for some voltage-gated properties, we measured firing properties and voltage-gated currents and developed a model for a homogeneous population of mouse basal neurons. For patch-clamp experiments, we used a mouse coronal VNO slice preparation that has the advantage, extensively exploited by previous studies (Leinders-Zufall *et al.*, 2000, 2004; Lucas *et al.*, 2003), of preserving the VNO cross-sectional structure and the possibility to distinguish between basal and apical cells, while dissociation procedures always destroy the native cellular topography. The experimentally measured electrical properties of basal mouse vomeronasal sensory neurons were used to estimate parameters necessary to implement ion channels in the model. Initial parameters were further refined until a good reproduction of both voltage-clamp and current-clamp data were obtained. The experimentally measured firing frequency as a function of injected current was exactly reproduced by the model.

Materials and methods

Preparation of acute slices of mouse VNO and patch-clamp recordings

Slices of the VNO were prepared from 30- to 90-day-old 129/Sv mice. Experiments were performed according to both international and Italian guidelines for the use of experimental animals. The VNO was removed and rinsed in chilled Ringer's solution (Figure 1A). The capsule and all cartilaginous tissues were carefully removed and the two halves of the VNO were isolated from the vomer bone. Each half of the VNO was then separately treated. The VNO was embedded in 0.5% low-grade agar (A7002 Sigma, St. Louis, MO) prepared with 0.9% saline solution once the agar had cooled to 38°C (Figure 1B). Upon solidification, the agar block was fixed in a glass Petri dish—orienting the VNO perpendicular to the blade—in preparation for slicing with a vibratome (Vibratome 1000 Plus Sectioning System, St Louis, MO). Coronal cross-sections of the VNO 250 μm in thickness were cut using a Teflon-coated blade (Personna, American Safety Razor Company, VA) in oxygenated Ringer solution (Figure 1C). Slices, embedded in their agar support, were then left to recover for >30 min before electrophysiological experiments were initiated. Slices were viewed with an upright microscope (Olympus BX51WI, Tokyo, Japan) by infrared differential contrast optics with water immersion 10× or 40× objectives. The murine slice preparation maintained the VNO cross-sectional structure, many individual neurons could be clearly distinguished by their morphology (Figure 1D), and it was possible to distinguish between basal and apical neurons. Vomeronasal sensory neurons on the surface of the slice preparation were easily accessible to patch-clamp recording, while cells below the surface were much more difficult to reach as the vomeronasal sensory epithelium has an elastic consistency. Whole-cell patch-clamp recordings were

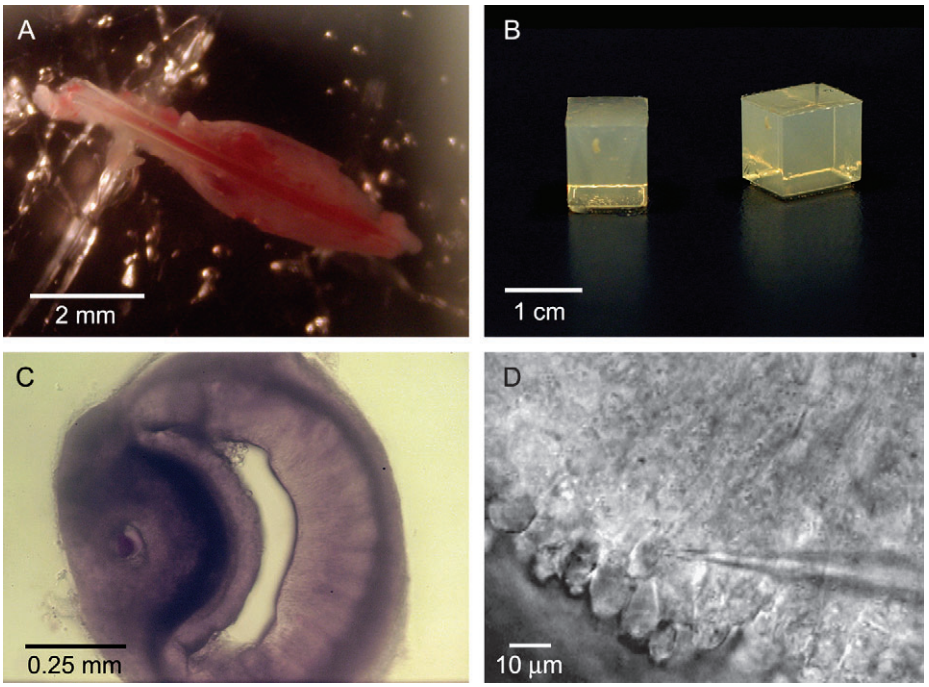

Figure 1 Preparation of mouse VNO coronal slices. **(A)** Top view of the intact, bilateral, capsule encased VNO freshly extracted from the mouse. **(B)** The capsule was removed and each half of the VNO was embedded vertically and perpendicular to the anticipated blade axis in preparation for sectioning. **(C)** A 250-µm thick coronal slice through the VNO with intact morphology. **(D)** Vomeronasal sensory neurons in the sensory epithelium of the acute slice preparation and patch pipette in preparation for electrophysiological recordings.

obtained by patching the soma of basal cells on the surface of the slice. Once in whole-cell configuration, it was possible to make continuous recordings for up to 2 h.

The recording chamber was continuously perfused with oxygenated Ringer solution by gravity flow. The slice was anchored to the base of the recording chamber using a home-made U-shaped platinum wire fitted with nylon threads ~3-mm apart from one another, thereby holding down the agar support without touching the slice itself. The Ringer solution contained (in mM) 125 NaCl, 2.5 KCl, 26 $NaHCO_3$, 1.25 NaH_2PO_4, 1.0 $MgCl_2$, 2.0 $CaCl_2$, 4.5 glucose, pH 7.4 oxygenated with 95% O_2, and 5% CO_2. Some experiments were made with the addition of 1 µM tetrodotoxin (TTX, Tocris, Ellisville, MO) or 10 mM tetraethylammonium (TEA) to the extracellular solution.

The whole-cell patch-clamp technique was used under voltage-clamp or current-clamp configurations using a Multiclamp 700B amplifier (Axon Instruments, La Jolla, CA). A Digidata 1200 analog to digital converter was used to interface the amplifier with a PC running pClamp 9.2 (Axon Instruments). Currents were low-pass filtered at 10 kHz and sampled at 20 kHz. Pipettes were pulled from glass capillaries (PG10165-4, World Precision Instruments, Sarasota, FL) using a two-stage Narishige puller (model PP-830, Narishige, Tokyo, Japan). The intracellular pipette solution contained (in mM) 145 KCl, 4 $MgCl_2$, 10 mM 4-2-hydroxyethyl-1-piperazine ethanesulfonic acid hemisodium, 0.5 ethylene glycol-bis(aminoethyl ether)-tetraacetic acid, 1 adenosine triphosphate, and 0.1 guanosine triphosphate, pH 7.4. Pipettes had a typical bath resistance of 3–6 MΩ when filled with the intracellular solution. Leakage and capacitive currents were not subtracted from currents under voltage clamp. Resting membrane potential was measured as the potential at which the current was zero. Input resistance was measured as the slope of linear current–voltage relationship around −80 mV. Cell membrane capacitance was measured by integrating the capacitive current transient elicited by a 10-mV hyperpolarizing step from a holding potential of −70 mV (Bigiani and Roper, 1993; Vogalis *et al.*, 2005). Experiments were conducted at room temperature 20–23°C. All chemicals were from Sigma unless otherwise stated.

Data analysis was performed using PClamp 9.2 software (Axon Instruments) and Igor 4.0 software (Wavemetrics, Lake Oswego, OR).

A previous study has shown that in some strains there could be a small difference in voltage-gated properties between vomeronasal sensory neurons of male and female (Dean *et al.*, 2004); however, in the mouse strain used in this study, no significant difference was found between sexes and therefore all data were pooled together.

Data are given as mean ± standard deviation and the total number of observations (*N*).

Model

All the simulations were carried out using NEURON, a simulation program for modeling neurons originally

developed by Michael Hines and John Moore and available for free download at http://neuron.duke.edu/. Version 5.7 of NEURON (Hines and Carnevale, 1997) was used with its variable time step feature. The model and simulation files for mouse vomeronasal sensory neurons originated from this work are available for public download under the ModelDB section of the Senselab database (http://senselab.med.yale.edu).

Morphologically, a model basal vomeronasal sensory neuron was implemented in the simulation program as composed of a somatic compartment and a dendrite of cylindrical shape. The mouse basal neuron was modeled with a soma of 14×14 μm and a dendrite of 70×1.5 μm, and the calculated membrane surface area was approximately 945 μm^2. The size of the model neuron is in general agreement with the average measurements previously published for dissociated neurons (Liman and Corey, 1996; Fieni *et al.*, 2003; Dean *et al.*, 2004). Since these neurons have a very high input resistance (1–18 GΩ, see Results), they are electrotonically very compact, and the entire neuron can be considered isopotential. Uniform passive properties were used, with the standard value for the specific membrane capacitance of 1 $\mu F/cm^2$, axial resistivity of 150 Ω·cm, specific membrane resistance of 155 $k\Omega \cdot cm^2$, and membrane time constant of 155 ms, based on the experimental estimation of the passive cell properties (see Results). Resting potential was set at −70 mV and temperature at 22°C.

Active properties included a sodium and a potassium current that were implemented using an Hodgkin and Huxley-like formalism (Johnston and Wu, 1995) as:

$$I_{\text{ion}} = g_{\max} m^n h (V - E_{\text{ion}}), \quad (1)$$

where I_{ion} is the Na^+ or K^+ current and, for each ion, $g_{\max}$ is the peak conductance, E_{ion} is the reversal potential, and m and h are the activation and inactivation gate variables, respectively. The steady-state (*ss*) voltage dependence of m and h was implemented using simple Boltzmann functions:

$$m_{ss} = \frac{1}{1 + \exp\left(\frac{V_{m,1/2} - V}{k_m}\right)}, \quad (2)$$

$$h_{ss} = \frac{1}{1 + \exp\left(\frac{V - V_{h,1/2}}{k_h}\right)}, \quad (3)$$

and the time constant to reach steady-state (τ_{ss}) was implemented using the following arbitrary function:

$$\tau_{ss\_x} = \frac{a_x \exp(z_x \gamma_x (V - V_{ss\_x}))}{1 + \exp(z_x (V - V_{ss\_x}))}, \quad (4)$$

where, for each ion, x is the gating variable (m or h), a_x is a parameter controlling the maximum τ_{ss_x} value, z_x its location on the voltage axis, and γ_x the degree of curve symmetry. Parameter values were chosen in such a way to have a good reproduction of both voltage- and current-clamp experiments. The final parameter values used in the simulation are reported in Table 1.

Results

The aim of this study was to generate a model of the electrical activity of vomeronasal sensory neurons that reproduces both the firing behavior and the overall voltage-gated properties of inward and outward currents. To implement this model, we used the simulation program NEURON, and we experimentally determined the electrical properties of basal vomeronasal sensory neurons. Experiments were performed using the whole-cell current-clamp and voltage-clamp configurations to record from individual basal neurons in mouse VNO slice preparations. Initial parameters were introduced in the model and, with a method of trial and error, we modified the model parameters, until a good reproduction of both our current-clamp and voltage-clamp data were obtained.

Passive properties

The resting potential of basal vomeronasal sensory neurons ranged from −50 to −70 mV, averaging −63 ± 6 mV (N = 16). The average capacitance was 12 ± 5 pF (range: 4–21 pF, N = 16), and the average input resistance (R_i) was 7 ± 5 GΩ (N = 16), with a range between 1 and 18 GΩ. Since seal resistances are usually a few gigaohms (with occasional higher values up to 50 GΩ), and therefore, are similar to the input resistance, in most recordings, R_i is likely to underestimate the real membrane resistance (R_m) (Schild, 1989; Schild and

Table 1 Model parameters used for the simulations of the electrical behavior of a mouse basal vomeronasal sensory neuron

Parameter	Na^+	K^+
n	3	1.5
$g_{\text{ion\_max}}$	11.4 mS/cm^2	2.1 mS/cm^2
E_{ion}	50 mV	−75 mV
$V_{m,1/2}$	−42 mV	−21 mV
k_m	8 mV	12.8 mV
a_m	3.3 ms	333.3 ms
V_{ss_m}	−38.9 mV	−75 mV
z_m	0.05 mV^{-1}	0.0002 mV^{-1}
γ_m	0.2	0.82
$V_{h,1/2}$	−60 mV	0 mV
k_h	2 mV	60 mV
a_h	33.3 ms	500 ms
V_{ss_h}	−80 mV	−70 mV
z_h	0.09 mV^{-1}	0.05 mV^{-1}
γ_h	0.5	0.95

Parameters for Na^+ and K^+ channels were defined in equations (1–4; 6–8).

Restrepo, 1998). Therefore, it is likely that R_m is closer to the higher measured value of R_i (18 GΩ) rather than to the mean value.

Firing behavior

The firing behavior of mouse basal vomeronasal sensory neurons in the acute slice preparation was investigated through whole-cell current-clamp recordings. Of 25 basal neurons, 15 fired repetitive action potentials in response to depolarizing current injections of 1–3 pA and four of them also showed spontaneous firing at 0 pA current injection. In some cases (N = 5), basal vomeronasal sensory neurons fired only 1 action potential, irrespective of the amount of current applied. The remaining neurons (N = 6) did not show any action potential. The generation of steady trains of action potentials with little sign of adaptation in most neurons is in agreement with previous studies in the mouse VNO (Liman and Corey, 1996) and was further examined in more detail. Figure 2A illustrates the tonic firing pattern of a representative basal vomeronasal sensory neuron in response to current injections from 2 to 10 pA. We calculated the spike duration as the width at 50% of the spike amplitude and found that the average spike duration at 2 pA was 13 ± 6 ms (range: 5–22 ms, N = 15). The tonic firing rate at 2 pA varied among neurons between 2 and 4 Hz (N = 15). The firing rate as a function of the injected current was plotted from a complete set of data from four basal vomeronasal sensory neurons in Figure 2B and fitted by a Michaelis–Menten equation:

$$F = \frac{F_{max} I}{I + I_o}, \quad (5)$$

where F is the firing frequency, I is the injected current, F_{max} is the maximal firing frequency, and I_o is the injected current producing half of the maximal firing frequency. The best fit of equation (5) to the data was obtained with F_{max} = 12 Hz and I_o = 7.5 pA.

Voltage-gated currents

To obtain an estimate of model parameters for voltage-gated currents, we measured inward and outward currents in the whole-cell voltage-clamp configuration. It has been previously shown in dissociated mouse vomeronasal sensory neurons that the voltage-gated inward current is primarily a sodium current, largely due to a TTX-sensitive component, although a TTX-insensitive sodium current component and calcium currents are also present (Liman and Corey, 1996; Fieni *et al.*, 2003). These previous studies have also shown that the voltage-gated outward currents are primarily composed of a potassium current sensitive to blockage by TEA, although also a smaller component that is not sensitive to TEA is present (Liman and Corey, 1996; Fieni *et al.*, 2003). We have measured inward and outward currents using standard protocols (Figures 3, 5, and 6) and confirmed

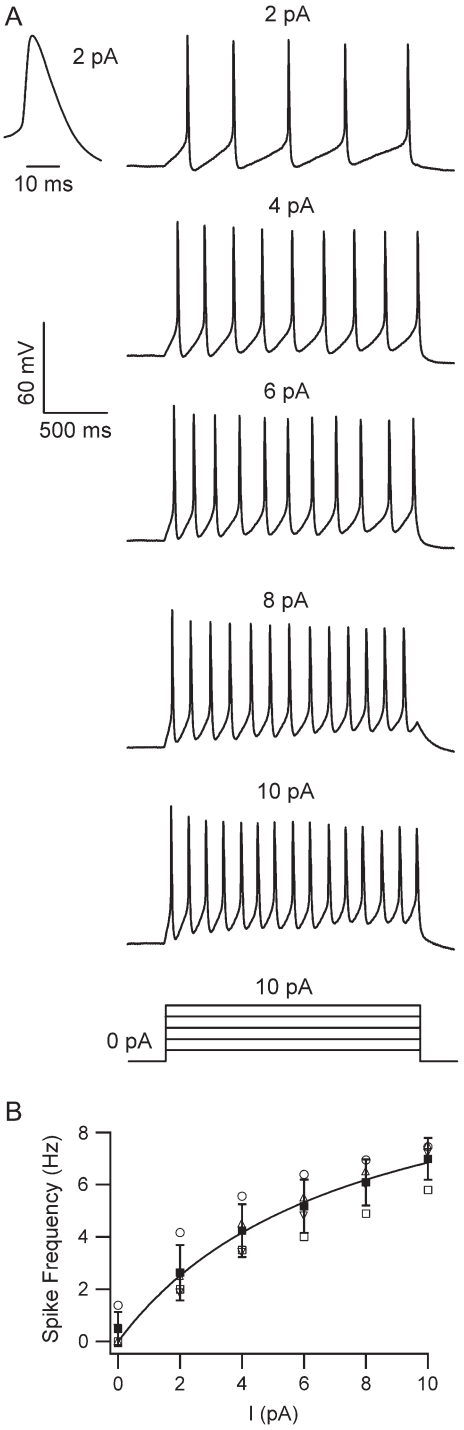

Figure 2 Firing patterns of a basal vomeronasal sensory neuron recorded from a mouse VNO slice. **(A)** Typical current-clamp responses to current injections of 2–10 pA for 2 s. In this neuron, the resting potential (measured at 0 pA current injection) was −70 mV. The firing frequency increased as a function of injected current. The inset at the top left shows a single action potential upon 2 pA current injection at an expanded time scale. Spike duration was 9 ms. **(B)** Firing frequency as a function of current injection for four neurons. Each neuron was represented by a different symbol. The black squares show the average ± standard deviation. The line was the best fit of the Michaelis–Menten equation (5) to the data with F_{max} = 12 Hz, I_o = 7.5 pA.

that the majority of inward current was blocked by 1 μM TTX (87% block at −15 mV, N = 3, data not shown) and that the outward current was largely abolished by 10 mM TEA (68% block at +30 mV, N = 4, data not shown). Therefore, in a first approximation and to obtain a model with a minimum number of parameters, we have tried to implement our model by determining the properties of voltage-gated currents as composed by one main type of sodium and potassium channels.

We measured the voltage dependences of activation and inactivation of inward and outward currents. For activation, inward currents were elicited by applying depolarizing voltage steps of 50-ms duration from the holding potential to a test potential between −60 to +35 mV (Figure 3A). Peak currents at each voltage were measured and plotted in Figure 3B as a function of the test potential for two holding potentials, −70 or −60 mV. Figure 3C shows the calculated normalized conductances plotted as a function of voltage. The activation parameters, which were subsequently used as initial values in the model, were estimated by fitting the data with the following equation:

$$\frac{g_{\mathrm{Na}}(V)}{g_{\mathrm{Na\_max}}} = \frac{1}{\left[1+\exp\left(\frac{V_{m,1/2}-V}{k_m}\right)\right]^n}, \qquad (6)$$

where g_{Na} is the sodium conductance, $g_{\mathrm{Na\_max}}$ is the maximum sodium conductance, $V_{m,1/2}$ is the half-activation potential of a simple Boltzmann equation (2), k_m is a slope constant, and n was 3 as in the Hodgkin–Huxley model. At a holding potential of −70 mV, the average $V_{m,1/2}$ was −44.7 ± 12.1 mV and k_m was 3.7 ± 2.1 mV (N = 3). Similar values were obtained at −60 mV, where the average $V_{m,1/2}$ was −42.5 ± 4.7 mV and k_{m} was 5.7 ± 2.5 mV (N = 20). Maximal peak values of the inward current were elicited at voltage steps between −30 and −10 mV and ranged from −1390 to −179 pA with a mean value of −778 ± 335 pA (N = 20).

To measure the inactivation properties of the sodium channels, the steady-state voltage dependence of inactivation was estimated by using a two-pulse protocol, as shown in Figure 4A. First, the neuron was held for 300 ms at voltages from −100 to −20 mV to achieve steady-state inactivation of sodium channels and then a test pulse to 0 mV was given to elicit the residual current that had not been inactivated. Peak currents were normalized to the maximal value and plotted as a function of the pre-pulse voltage in Figure 4B. The inactivation parameters were estimated by fitting the data with the following equation:

$$\frac{I(V)}{I_{\max}} = \frac{1}{1+\exp\left(\frac{V-V_{h,1/2}}{k_h}\right)}, \qquad (7)$$

where I is the peak current measured at the pre-pulse voltage V, $I_{\max}$ is the maximal peak current, $V_{h,1/2}$ is the half-activation pre-pulse voltage, and k_h is the slope constant. The average $V_{h,1/2}$ was −56.2 ± 7.2 mV and k_h was 8.9 ± 2.3 mV (N = 14).

The kinetics of activation and inactivation of sodium currents were fit by a single exponential and found to be very fast: at 0 mV, the average time constants of activation and inactivation were 0.6 ± 0.3 and 0.9 ± 0.3 ms (N = 11), respectively.

Properties of outward currents were estimated as shown in Figure 5. Currents in response to step depolarizations of 400-ms duration from a holding potential of −60 mV are shown in Figure 5. The outward currents showed little inactivation over 400 ms. Peak outward currents and normalized conductances are plotted as a function of voltage

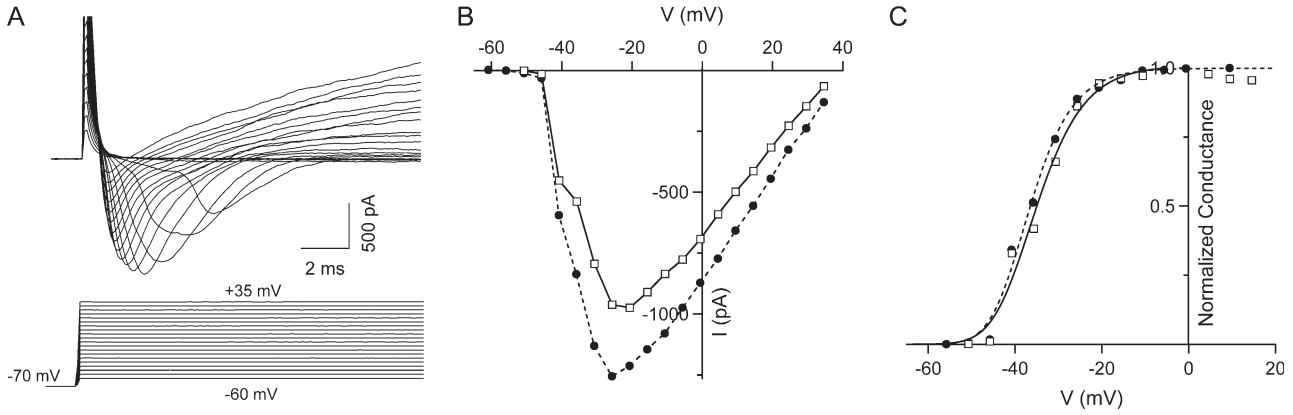

Figure 3 Activation properties of inward currents. **(A)** Voltage-clamp recordings from a basal vomeronasal sensory neuron from a mouse VNO slice. Current traces measured as the voltage was stepped in increments of 5 mV from −60 to +35 mV from a holding potential of −70 mV. **(B)** Current-voltage relationships of the peak inward currents measured in the same neuron at the holding potential of −70 mV (circles) or −60 mV (squares). **(C)** Steady-state activation curve. Normalized conductances from data in (B) were plotted as a function of voltage. Activation curves were fit with equation (6). At a holding potential of −70 mV (circles and broken line), $V_{m,1/2}$ = −44.6 mV and k_m = 6.0 mV. At a holding potential of −60 mV (squares and continuous line), $V_{m,1/2}$ = −43.9 mV and k_m = 6.7 mV.

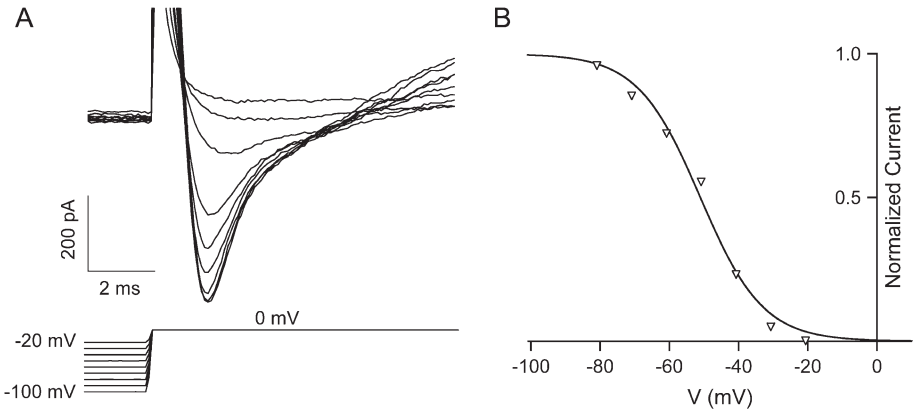

Figure 4 Inactivation properties of inward currents. **(A)** Inward currents elicited by a test pulse of 0 mV following the application of a 300 ms pre-pulse at the indicated voltages from −100 to −20 mV. **(B)** Peak currents were normalized to the maximal current and plotted as a function of the pre-pulse potential. The inactivation curve was fit using equation (7) where $V_{h,1/2}$= −51.1 mV and k_h = 9.0 mV.

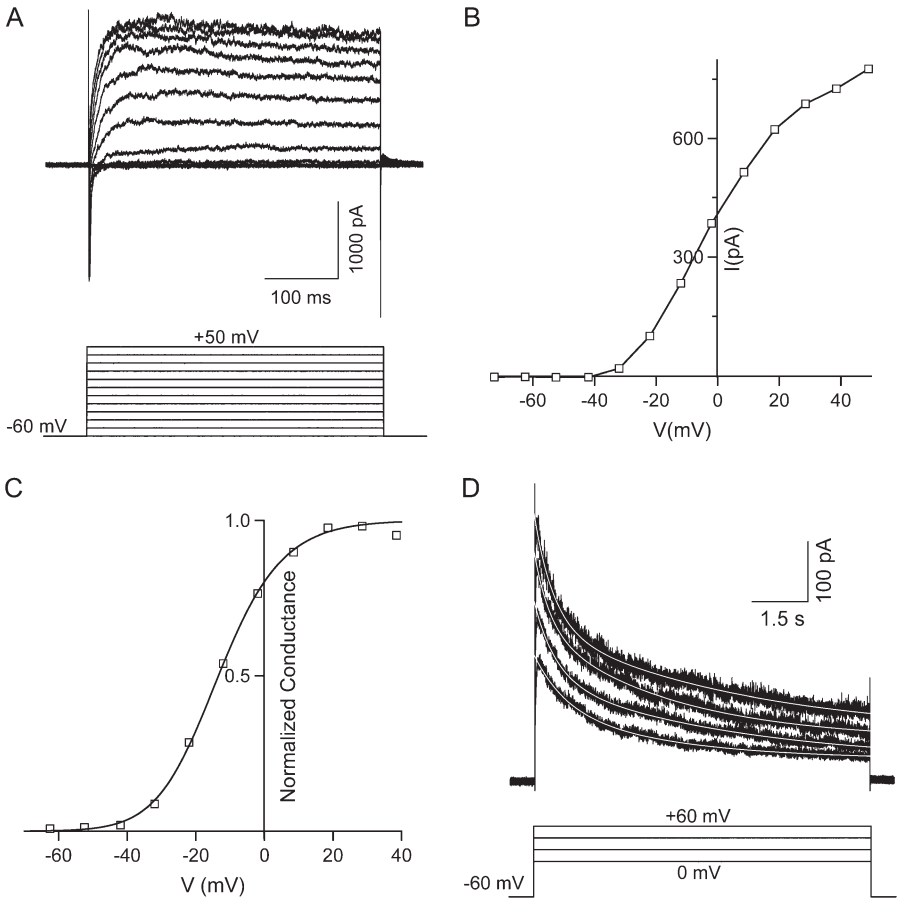

Figure 5 Activation and inactivation of outward currents. **(A)** Currents elicited by a 400-ms voltage pulse in steps of 10 mV from −60 to +50 mV from a holding potential of −60 mV. **(B)** Current–voltage relationship of the peak outward currents. **(C)** Outward current steady-state activation curve. Normalized conductances from data in (B) were plotted as a function of voltage. The activation curve was fit using equation (8) with $V_{m,1/2}$= −18.8 mV, k_m = 10.2 mV. **(D)** Inactivation of potassium current. Voltage steps of 9-s duration and 20-mV amplitude from 0 to +60 mV were applied from a holding potential of −60 mV. Solid white lines represent the fit of the data with a double exponential function with time constants of 0.8 and 3 s for the fast and slow components, respectively, at 0 mV, 0.6 s, and 5 s at +20 mV, 0.4 and 4 s at +40 mV, and 0.5 and 5 s at +60 mV.

in Figure 5B and C, respectively. The steady-state activation curve for potassium was fit with the equation:

$$\frac{g_K(V)}{g_{K\_max}} = \frac{1}{\left[1+\exp\left(\frac{V_{m,1/2}-V}{k_m}\right)\right]^n}, \quad (8)$$

where g_K is the potassium conductance, g_{K_max} is the maximum potassium conductance, $V_{m,1/2}$ is the half-activation potential for a simple Boltzmann equation (2), k_m is a slope constant, and n is 1.5 (n was determined using the Hodgkin–Huxley model as a starting point and modified to provide an accurate representation of the model currents). At a holding potential of −60 mV, the average $V_{m,1/2}$ was −21.0 ± 4.9 mV and k_m was 12.8 ± 2.4 mV (N = 19). Maximal peak values of the outward current measured at voltage steps of +50 mV ranged from 210 to 1295 pA with a mean value of 635 ± 279 pA (N = 19).

The kinetics of activation of potassium currents were fit by a single exponential and were slower than those for sodium: at 0 mV, the time constant of activation was 16.3 ± 6.4 ms (N = 19). The kinetics of inactivation were further investigated with step depolarizations of 9-s duration (Figure 4D). Inactivation of outward currents was very slow and was fit by a double exponential function: at 0 mV, the average time constants of inactivation were 0.9 ± 0.8 and 4.0 ± 2.1 s (N = 4).

Model

The experimentally determined parameters were used as initial values in the model of a vomeronasal sensory neuron and were then adjusted to closely reproduce both voltage-clamp and current-clamp experiments. The electrical behavior of a model neuron is illustrated in Figures 6 and 7, and the final parameter values are reported in Table 1.

Figure 6 shows a comparison between simulations modeling voltage-gated currents and experimental recordings. Traces represent currents evoked by voltage steps from −60 mV to +30 mV in 10 mV increments from a holding potential of −70 mV. The maximal peak inward current occurred at −20 mV for both experimental (Figure 6A) and modeled (Figure 6B) currents. The overall current properties are quite well reproduced by the model.

Figure 7 shows modeled action potentials, whose amplitude and firing frequency also closely resembled the experimental findings under current clamp (Figure 2). The firing frequency obtained in the model was plotted as a function of the injected current in Figure 7B, and the best fit of equation (5) to the data yielded the same values, F_{max} = 12 Hz and I_o = 7.5 pA, obtained with experimental data (Figure 2B). The spike duration at 2 pA in the model neuron was slightly shorter, 6 ms, than in the experimental recordings shown in Figure 2A, where a spike duration of 9 ms was measured. However, modification of the potassium conductance in such a way to increase the spike duration resulted in the loss of accurate firing frequency and outward current response.

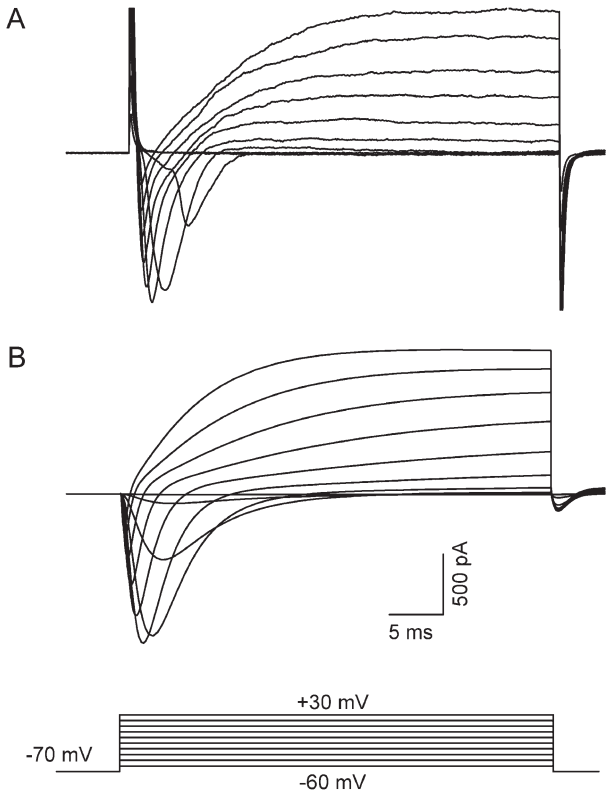

Figure 6 Experimental and simulated voltage-clamp recordings from a basal vomeronasal sensory neuron. **(A)** Voltage-clamp recordings were obtained from a holding potential of −70 mV by voltage steps from −60 to +30 mV in 10 mV increments. **(B)** Simulation of the same type of voltage-clamp experiment as shown in (A) in a model vomeronasal sensory neuron. Parameters used in the model are listed in Table 1.

In summary, a comparison between Figures 2, 6, and 7 shows that the model of the electrical activity of a mouse basal vomeronasal sensory neuron presented here well reproduces the voltage-clamp data and the generation of action potentials as a function of current injection.

Conclusion

In this study, we developed a model of the electrical behavior of basal mouse vomeronasal sensory neurons based on electrophysiological data obtained with the whole-cell voltage-clamp and current-clamp configurations from VNO slices. To our knowledge, the only published model of vomeronasal sensory neuron activity is an elegant, remarkably simple, quantitative model of ligand binding (Holy *et al.*, 2000), capable of capturing the time course of the VNO spiking responses to chemical stimuli. Holy *et al.* (2000) based their model on the experimental observations, obtained with extracellular multi-array recordings, that vomeronasal sensory neurons showed little or no adaptation to chemical stimuli and therefore that the average firing rate could directly represent the occupancy of a pheromone receptor, as determined by the first-order binding kinetics. Here the goal was

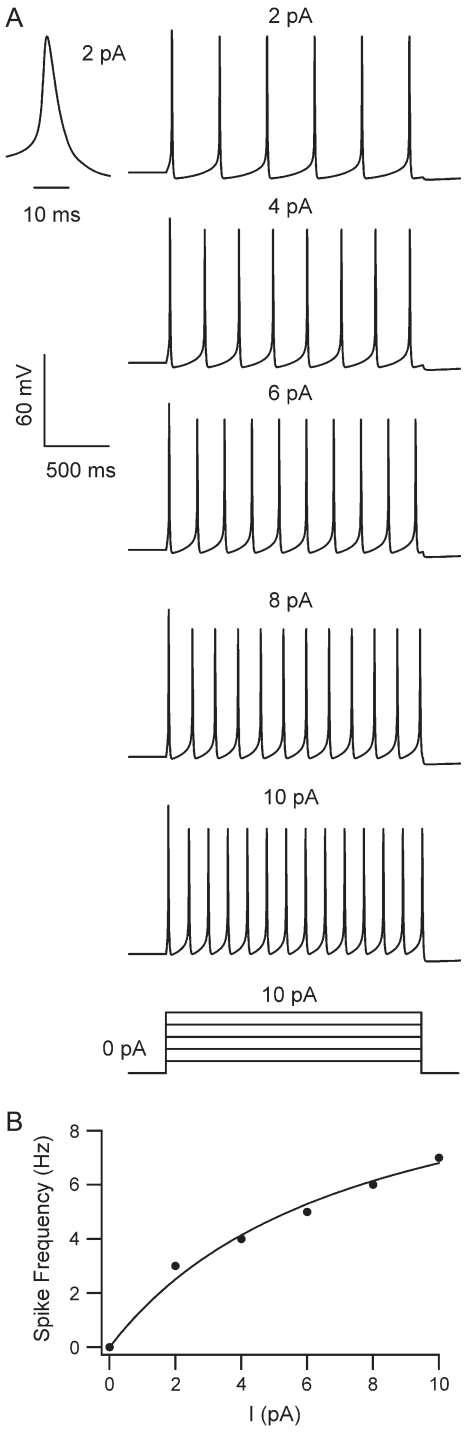

Figure 7 Simulated firing properties of the model basal vomeronasal sensory neuron. **(A)** The holding potential was set to −70 mV, and current-clamp experiments as those shown in Figure 2A were modeled. Model parameters are listed in Table 1. The firing frequency increased as a function of current injection in a manner similar to that observed experimentally. The inset at the top left shows the model of a single action potential upon 2 pA current injection at an expanded time scale. Spike duration was 6 ms. **(B)** Firing frequency as a function of current injection calculated from the model. The simulated data were fit with a Michaelis–Menten equation (5) with F_{max} = 12 Hz, I_o = 7.5 pA as in the experimental recordings of Figure 2B.

different: to develop a simple model of vomeronasal sensory neurons capable of reproducing the firing activity that occurs after the vomeronasal transduction cascade based on the properties of the voltage-gated membrane ion channels underlying the generation of action potentials. This model could be used in combination with future models that will include details of the transduction cascade of basal vomeronasal sensory neurons. We have chosen to find a model with a minimal number of parameters that could reproduce our experimental data and, especially, the most important property for signal transmission, the firing behavior. We were able to obtain quantitative agreement with experiments by using only one type of sodium and potassium channels, each one of them closely based on the two main currents measured in these neurons. The firing frequency as a function of injected current was exactly reproduced by our model, although the exact action potential shape was not perfectly reproduced. Given the agreement between experimental and modeled firing properties, we consider the exact shape of a single action potential a very minor problem at this stage with a negligible effect (if any) on the overall input–output characteristics. We conclude that this first model, although far from being complete and requiring additional refinements, represents a good quantitative model of the electrical activity of basal vomeronasal sensory neurons, effectively mimicking the information passed to the brain—the firing pattern.

Acknowledgements

This work was supported by grants NFG 503221 from the European Community and COFIN 2004 from the Italian Ministry of Education, Research and University.

References

Berghard, A. and **Buck, L.B.** (1996) *Sensory transduction in vomeronasal neurons: evidence for G alpha o, G alpha i2, and adenylyl cyclase II as major components of a pheromone signaling cascade.* J. Neurosci., 16, 909–918.

Bigiani, A., Mucignat-Caretta, C., Montani, G. and **Tirindelli, R.** (2005) *Pheromone reception in mammals.* Rev. Physiol. Biochem. Pharmacol., 10.1007/S10254-004-0038-00.

Bigiani, A. and **Roper, S.D.** (1993) *Identification of electrophysiologically distinct cell subpopulations in Necturus taste buds.* J. Gen. Physiol., 102, 143–170.

Boschat, C., Pelofi, C., Randin, O., Roppolo, D., Luscher, C., Broillet, M.C. and **Rodriguez, I.** (2002) *Pheromone detection mediated by a V1r vomeronasal receptor.* Nat. Neurosci., 5, 1261–1262.

Brennan, P.A. and **Keverne, E.B.** (2004) *Something in the air? New insights into mammalian pheromones.* Curr. Biol., 14, R81–R89.

Cinelli, A.R., Wang, D., Chen, P., Liu, W. and **Halpern, M.** (2002) *Calcium transients in the garter snake vomeronasal organ.* J. Neurophysiol., 87, 1449–1472.

Dean, D.M., Mazzatenta, A. and **Menini, A.** (2004) *Voltage-activated current properties of male and female mouse vomeronasal sensory neurons: sexually dichotomous?* J. Comp. Physiol. A Neuroethol. Sens. Neural Behav. Physiol., 190, 491–499.

Del Punta, K., Leinders-Zufall, T., Rodriguez, I., Jukam, D., Wysocki, C.J., Ogawa, S., Zufall, F. and **Mombaerts, P.** (2002) *Deficient pheromone responses in mice lacking a cluster of vomeronasal receptor genes.* Nature, 419, 70–74.

Døving, K.B. and **Trotier, D.** (1998) *Structure and function of the vomeronasal organ.* J. Exp. Biol., 201, 2913–2925.

Dulac, C. and **Axel, R.** (1995) *A novel family of genes encoding putative pheromone receptors in mammals.* Cell, 83, 195–206.

Dulac, C. and **Torello, A.T.** (2003) *Molecular detection of pheromone signals in mammals: from genes to behaviour.* Nat. Rev. Neurosci., 4, 551–562.

Fadool, D.A., Wachowiak, M. and **Brann, J.H.** (2001) *Patch-clamp analysis of voltage-activated and chemically activated currents in the vomeronasal organ of* Sternotherus odoratus *(stinkpot/musk turtle).* J. Exp. Biol., 204, 4199–4212.

Fieni, F., Ghiaroni, V., Tirindelli, R., Pietra, P. and **Bigiani, A.** (2003) *Apical and basal neurones isolated from the mouse vomeronasal organ differ for voltage-dependent currents.* J. Physiol., 552, 425–436.

Ghiaroni, V., Fieni, F., Tirindelli, R., Pietra, P. and **Bigiani, A.** (2003) *Ion conductances in supporting cells isolated from the mouse vomeronasal organ.* J. Neurophysiol., 89, 118–127.

Halpern, M. and **Martinez-Marcos, A.** (2003) *Structure and function of the vomeronasal system: an update.* Prog. Neurobiol., 70, 245–318.

Herrada, G. and **Dulac, C.** (1997) *A novel family of putative pheromone receptors in mammals with a topographically organized and sexually dimorphic distribution.* Cell, 90, 763–773.

Hines, M.L. and **Carnevale, N.T.** (1997) *The NEURON simulation environment.* Neural Comput., 9, 1179–1209.

Holy, T.E., Dulac, C. and **Meister, M.** (2000) *Responses of vomeronasal neurons to natural stimuli.* Science, 289, 1569–1572.

Inamura, K. and **Kashiwayanagi, M.** (2000) *Inward current responses to urinary substances in rat vomeronasal sensory neurons.* Eur. J. Neurosci., 12, 3529–3536.

Inamura, K., Kashiwayanagi, M. and **Kurihara, K.** (1997) *Inositol-1,4,5-trisphosphate induces responses in receptor neurons in rat vomeronasal sensory slices.* Chem. Senses, 22, 93–103.

Inamura, K., Matsumoto, Y., Kashiwayanagi, M. and **Kurihara, K.** (1999) *Laminar distribution of pheromone-receptive neurons in rat vomeronasal epithelium.* J. Physiol., 517(Pt 3), 731–739.

Jacobson, L., Trotier, D. and **Døving, K.B.** (1998) *Anatomical description of a new organ in the nose of domesticated animals by Ludvig Jacobson (1813).* Chem. Senses, 23, 743–754.

Jia, C. and **Halpern, M.** (1996) *Subclasses of vomeronasal receptor neurons: differential expression of G proteins (Gi alpha 2 and G(o alpha)) and segregated projections to the accessory olfactory bulb.* Brain Res., 719, 117–128.

Johnston, D. and **Wu, S.M.** (1995) Foundations of Cellular Neurophysiology. MIT Press, Cambridge, MA.

Keverne, E.B. (2002) *Mammalian pheromones: from genes to behaviour.* Curr. Biol., 12, R807–R809.

Labra, A., Brann, J.H. and **Fadool, D.A.** (2005) *Heterogeneity of voltage- and chemosignal-activated response profiles in vomeronasal sensory neurons.* J. Neurophysiol., 94, 2535–2548.

Leinders-Zufall, T., Brennan, P., Widmayer, P., Chandramani, P.S., Maul-Pavicic, A., Jager, M., Li, X.H., Breer, H., Zufall, F. and **Boehm, T.** (2004) *MHC class I peptides as chemosensory signals in the vomeronasal organ.* Science, 306, 1033–1037.

Leinders-Zufall, T., Lane, A.P., Puche, A.C., Ma, W., Novotny, M.V., Shipley, M.T. and **Zufall, F.** (2000) *Ultrasensitive pheromone detection by mammalian vomeronasal neurons.* Nature, 405, 792–796.

Leypold, B.G., Yu, C.R., Leinders-Zufall, T., Kim, M.M., Zufall, F. and **Axel, R.** (2002) *Altered sexual and social behaviors in trp2 mutant mice.* Proc. Natl Acad. Sci. USA, 99, 6376–6381.

Liman, E.R. and **Corey, D.P.** (1996) *Electrophysiological characterization of chemosensory neurons from the mouse vomeronasal organ.* J. Neurosci., 16, 4625–4637.

Liman, E.R., Corey, D.P. and **Dulac, C.** (1999) *TRP2: a candidate transduction channel for mammalian pheromone sensory signaling.* Proc. Natl Acad. Sci. USA, 96, 5791–5796.

Lucas, P., Ukhanov, K., Leinders-Zufall, T. and **Zufall, F.** (2003) *A diacylglycerol-gated cation channel in vomeronasal neuron dendrites is impaired in TRPC2 mutant mice: mechanism of pheromone transduction.* Neuron, 40, 551–561.

Luo, M. and **Katz, L.C.** (2004) *Encoding pheromonal signals in the mammalian vomeronasal system.* Curr. Opin. Neurobiol., 14, 428–434.

Matsunami, H. and **Buck, L.B.** (1997) *A multigene family encoding a diverse array of putative pheromone receptors in mammals.* Cell, 90, 775–784.

Menco, B.P., Carr, V.M., Ezeh, P.I., Liman, E.R. and **Yankova, M.P.** (2001) *Ultrastructural localization of G-proteins and the channel protein TRP2 to microvilli of rat vomeronasal receptor cells.* J. Comp. Neurol., 438, 468–489.

Rodriguez, I. (2003) *Nosing into pheromone detectors.* Nat. Neurosci., 6, 438–440.

Rodriguez, I. (2004) *Pheromone receptors in mammals.* Horm. Behav., 46, 219–230.

Ryba, N.J. and **Tirindelli, R.** (1997) *A new multigene family of putative pheromone receptors.* Neuron, 19, 371–379.

Sam, M., Vora, S., Malnic, B., Ma, W., Novotny, M.V. and **Buck, L.B.** (2001) *Neuropharmacology. Odorants may arouse instinctive behaviours.* Nature, 412, 142.

Schild, D. (1989) *Whole-cell currents in olfactory receptor cells of* Xenopus laevis. Exp. Brain Res., 78, 223–232.

Schild, D. and **Restrepo, D.** (1998) *Transduction mechanisms in vertebrate olfactory receptor cells.* Physiol. Rev., 78, 429–466.

Spehr, M., Hatt, H. and **Wetzel, C.H.** (2002) *Arachidonic acid plays a role in rat vomeronasal signal transduction.* J. Neurosci., 22, 8429–8437.

Stowers, L., Holy, T.E., Meister, M., Dulac, C. and **Koentges, G.** (2002) *Loss of sex discrimination and male-male aggression in mice deficient for TRP2.* Science, 295, 1493–1500.

Taniguchi, M., Kashiwayanagi, M. and **Kurihara, K.** (1995) *Intracellular injection of inositol 1,4,5-trisphosphate increases a conductance in membranes of turtle vomeronasal receptor neurons in the slice preparation.* Neurosci. Lett., 188, 5–8.

Taniguchi, M., Kashiwayanagi, M. and **Kurihara, K.** (1996) *Intracellular dialysis of cyclic nucleotides induces inward currents in turtle vomeronasal receptor neurons.* J. Neurosci., 16, 1239–1246.

Taniguchi, M., Wang, D. and **Halpern, M.** (2000) *Chemosensitive conductance and inositol 1,4,5-trisphosphate-induced conductance in snake vomeronasal receptor neurons.* Chem. Senses, 25, 67–76.

Trinh, K. and **Storm, D.R.** (2003) *Vomeronasal organ detects odorants in absence of signaling through main olfactory epithelium.* Nat. Neurosci., 6, 519–525.

Trotier, D. and **Døving, K.B.** (1996) *Direct influence of the sodium pump on the membrane potential of vomeronasal chemoreceptor neurones in frog.* J. Physiol., 490, 611–621.

Trotier, D., Døving, K.B., Ore, K. and **Shalchian-Tabrizi, C.** (1998) *Scanning electron microscopy and gramicidin patch clamp recordings of microvillous receptor neurons dissociated from the rat vomeronasal organ.* Chem. Senses, 23, 49–57.

Trotier, D., Døving, K.B. and **Rosin, J.F.** (1993) *Voltage-dependent currents in microvillar receptor cells of the frog vomeronasal organ.* Eur. J. Neurosci., 5, 995–1002.

Vogalis, F., Hegg, C.C. and **Lucero, M.T.** (2005) *Ionic conductances in sustentacular cells of the mouse olfactory epithelium.* J. Physiol., 562, 785–799.

Zufall, F., Kelliher, K.R. and **Leinders-Zufall, T.** (2002) *Pheromone detection by mammalian vomeronasal neurons.* Microsc. Res. Tech., 58, 251–260.

Zufall, F., Ukhanov, K., Lucas, P. and **Leinders-Zufall, T.** (2005) *Neurobiology of TRPC2: from gene to behavior.* Pflugers Arch., 451, 61–71.

Accepted February 16, 2006